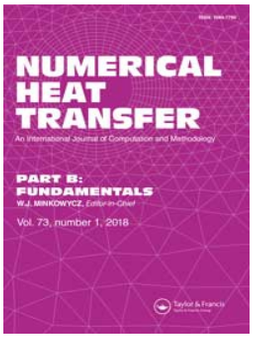

Taylor & Francis
Taylor & Francis Group

Numerical Heat Transfer, Part B: Fundamentals
An International Journal of Computation and Methodology

ISSN: 1040-7790 (Print) 1521-0626 (Online) Journal homepage: http://www.tandfonline.com/loi/unhb20

A hybrid flux splitting method for compressible flow

Shaolong Guo & Wen-Quan Tao

To cite this article: Shaolong Guo & Wen-Quan Tao (2018) A hybrid flux splitting method for compressible flow, Numerical Heat Transfer, Part B: Fundamentals, 73:1, 33-47, DOI: 10.1080/10407790.2017.1420315

To link to this article: https://doi.org/10.1080/10407790.2017.1420315

Published online: 16 Jan 2018.

NUMERICAL HEAT TRANSFER, PART B
2018, VOL. 73, NO. 1, 33–47
https://doi.org/10.1080/10407790.2017.1420315

A hybrid flux splitting method for compressible flow

Shaolong Guo and Wen-Quan Tao

Key Laboratory of Thermo-fluid Science and Engineering of MOE, School of Energy & Power Engineering, Xi'an Jiaotong University, Xi'an, China

ABSTRACT

A hybrid flux splitting scheme, called AUSM$^+$–FVS((advection upstream splitting method)$^+$–flux vector splitting), is proposed in this article to calculate the inviscid fluxes of Euler/Navier–Stokes equations. This new scheme is obtained by hybridizing the AUSM+ scheme with FVS method. When the local Mach number tends to zero, this scheme is similar to the AUSM+. Contrarily, this scheme is similar to the FVS at the shock region. Thus, this scheme has the accuracy of AUSM+ in boundary layer region and the robustness of FVS in shock region. Several numerical tests show that AUSM$^+$–FVS can reduce the shock instability and has a good accuracy in boundary layer region.

ARTICLE HISTORY
Received 11 October 2017
Accepted 12 December 2017

1. Introduction

Compressible flow problems are usually very complex, often containing shock waves and shock–shock interaction phenomena. Simulation of compressible fluid flow has been a big challenge over the years. Lots of numerical methods to predict the inviscid fluxes of Euler/Navier–Stokes (N–S) equations have been proposed. Among them, the upwind methods have been widely adopted. The commonly used upwind schemes include flux vector splitting (FVS) scheme, flux difference splitting (FDS) scheme, and advection upstream splitting method (AUSM)-type scheme. In the FVS scheme, the inviscid fluxes are split into upstream and downstream fluxes. Different splitting methods give rise to different FVS schemes, such as Steger and Warming splitting [1] and Van Leer splitting [2]. It is found that the FVS schemes are very robust and can capture the shock wave successfully. However, because of excessive numerical dissipation, the FVS schemes have a very poor accuracy in resolving the boundary layer region. In the FDS scheme, the flow between two adjacent grid units is regarded as a local Riemann problem which is based on Godunov's idea. The FDS scheme has shown its great capability of capturing the shock wave and contact discontinuity accurately. Those FDS schemes such as Roe's FDS [3] and Harten, Lax, van Leer and Einfeldt (HLLE) [4] can provide precise resolution in the boundary layer for viscous flow calculation. In the AUSM-type scheme [5], the inviscid flux vector is divided into convective part and pressure part. For the convective part, the upwind direction at the interface is decided by the sign of Mach number. Many researchers have pointed out that this method has both the efficiency of FVS and the accuracy of FDS [6]. This method was first proposed by Liou and Steffen [5]. After that, there are lots of developments, like advection upstream splitting method (AUSM)+ [7], advection upstream splitting method flux-Difference splitting-biased scheme (AUSMD) [8], advection upstream splitting method with pressure-based weight function (AUSMPW)+ [9], and AUSM$^+$-up [10]. All those are called AUSM-type scheme.

Although lots of shock-capturing methods as mentioned above have been proposed to obtain the inviscid fluxes of Euler/Navier–Stokes equations, there are still some unresolved problems of these schemes. When using the low-diffusion schemes such as Roe's FDS, AUSM, AUSM+, AUSMPW+,

CONTACT Wen-Quan Tao wqtao@mail.xjtu.edu.cn Key Laboratory of Thermo-fluid Science and Engineering of MOE, School of Energy & Power Engineering, Xi'an Jiaotong University, 28 Xian Ning Road, Xi'an 710049, Shannxi, China.
Color versions of one or more of the figures in the article can be found online at www.tandfonline.com/unhb.

Nomenclature

a	acoustic speed, m/s	y	Cartesian coordinate, m
e	total energy, J/kg	γ	specific heat ratio
H	enthalpy, J/kg	λ	thermal conductivity, $Wm^{-1}K^{-1}$
M	Mach number	μ	dynamic viscosity, Pa s
p	pressure, Pa	ρ	density, kg/m^3
q	heat flux, W/m^2	τ	time, s
T	temperature, K	***Subscripts***	
u	velocity in x-direction, m/s	f	fluid
v	velocity in y-direction, m/s	w	wall
w	velocity in z-direction, m/s	∞	freestream
x	Cartesian coordinate, m		

the results all suffer, to a certain extent, from spurious solutions of the shock in some situation, such as the carbuncle phenomenon and kinked Mach stem problem. In 1988, Peery and Imlay first named the carbuncle phenomenon when they simulated the hypersonic flow over a blunt body using Roe's scheme [11]. The carbuncle phenomenon often means a distorted bow shock prediction at the region ahead of the stagnation point. The kinked Mach stem problem can be shown in the double-Mach reflection problem [12]. Some characteristics about the carbuncle phenomenon are observed by Pandolfi and D'Ambrosio [13]. It is found that many factors can result in this phenomenon, such as flow Mach number, mesh geometry, and shock-capturing schemes. It is worth mentioning that the grid aspect ratio plays an important role in bringing about this phenomenon. The elongated mesh cell along the normal direction of the shock can exacerbate the shock instability [13]. The carbuncle phenomenon occurs more often in the first-order integration scheme, than in higher order reconstruction schemes [13]. Many investigations have been presented to reveal the causes and to solve this problem. Liou [14] examined lots of mass flux schemes and proposed the conjecture that if the mass flux scheme is not related to the pressure term, this scheme is free from the carbuncle solution. But this conjecture was disproved by other researchers later [15]. Ramalho et al. [16] found the numerical shock instabilities when using unstructured meshes in the computation which was contrary to Xu's observation [17]. Thus, as indicated in [18] there is still a lack of accepted explanations for the carbuncle phenomenon, and for the AUSM-type schemes, this key problem has not yet solved for the past quarter-century [19]. For the FVS schemes, according to Xie et al. [20], they are free from the shock instability. But, as mentioned above, they have a bad property in the boundary layer because of excessive dissipation.

To find a scheme which has both good accuracy and robustness, one way is to construct a scheme which possesses the accuracy of AUSM type and robustness of FVS. In this paper, a new scheme which hybridizes FVS scheme and AUSM+ scheme together, called AUSM$^+$–FVS for simplicity, is proposed to calculate the inviscid fluxes. To verify the accuracy and robustness of this new scheme, some classical numerical tests are studied.

In the following presentation, the 2-D compressible N–S equations will be presented, followed by the detailed description of the flux splitting schemes, including the new scheme proposed by this paper. Then the results of five numerical tests will be provided to show the robustness and the accuracy of the new scheme. Finally, some conclusion will be drawn.

2. Governing equations

The 2-D compressible N–S equations can be written as:

$$\frac{\partial \mathbf{U}}{\partial \tau}+\frac{\partial \mathbf{F}_1(\mathbf{U})}{\partial x}+\frac{\partial \mathbf{F}_2(\mathbf{U})}{\partial y}-\frac{\partial \mathbf{F}_{v1}(\mathbf{U})}{\partial x}-\frac{\partial \mathbf{F}_{v2}(\mathbf{U})}{\partial y}=0 \tag{1}$$

where $\mathbf{U}$ signifies the conserving variables. The vector in the present work is

$$\mathbf{U}=[\rho,\rho u,\rho v,\rho e]^T \tag{2}$$

Here, ρ is the density, u and v are the x and y components of the velocity, and e is the energy per unit volume. The inviscid fluxes $\mathbf{F}_1$ and $\mathbf{F}_2$ are

$$\begin{aligned}\mathbf{F}_1(\mathbf{U}) &= [\rho u, \rho u^2 + p, \rho v u, u\rho H]^T \\ \mathbf{F}_2(\mathbf{U}) &= [\rho v, \rho u v, \rho v^2 + p, v\rho H]^T\end{aligned} \tag{3}$$

where p is the pressure, H is the gas enthalpy. They are calculated as follows:

$$p = (\gamma - 1)\rho[e - (u^2 + v^2)/2] \tag{4}$$

$$H = \frac{\gamma}{\gamma - 1}\frac{p}{\rho} + \frac{1}{2}(u^2 + v^2) \tag{5}$$

The specific heat ratio γ is taken as 1.4 for the perfect gas. The viscous flux vectors are

$$\begin{aligned}\mathbf{F}_{\upsilon 1}(\mathbf{U}) &= [0, \sigma_{xx}, \sigma_{xy}, u\sigma_{xx} + v\sigma_{xy} - q_x]^T \\ \mathbf{F}_{\upsilon 2}(\mathbf{U}) &= [0, \sigma_{yx}, \sigma_{yy}, u\sigma_{yx} + v\sigma_{yy} - q_y]^T\end{aligned} \tag{6}$$

In Eq. (6), q_x and q_y are the x and y components of the heat flux, σ is the viscous stress tensor of the fluid.

3. Flux splitting method

It is well known that the upwind method has many advantages in numerical simulation, such as a good robustness and being consistent with the physical characteristics. The execution of this scheme for incompressible flow is very simple, but when using this method in the compressible flow simulation, the implementation is usually complicated and needs some special treatments. For example, for one-dimensional situation, Euler equations can be written as:

$$\frac{\partial \mathbf{U}}{\partial \tau} + \mathbf{A}\frac{\partial \mathbf{U}}{\partial x} = 0 \tag{7}$$

where $\mathbf{A}$ is the Jacobian matrix which can be defined as $\mathbf{A} = \partial\mathbf{F}(\mathbf{U})/\partial\mathbf{U}$. The matrix $\mathbf{A}$ can be decomposed as follows:

$$\mathbf{A} = \mathbf{L}\Lambda\mathbf{R} \tag{8}$$

where $\mathbf{L}$ is the left eigenvector, $\mathbf{R}$ is the right eigenvector, and $\mathbf{\Lambda}$ is the eigenvalue matrix which is

$$\mathbf{\Lambda} = \begin{bmatrix} u & 0 & 0 \\ 0 & u - a & 0 \\ 0 & 0 & u + a \end{bmatrix} \tag{9}$$

The eigenvalues of Jacobian matrix are $\lambda_1 = u$, $\lambda_2 = u - a$, $\lambda_3 = u + a$. Here, a is the acoustic speed. When $|u| < a$, the signs of the three eigenvalues are not the same which means that the waves have different propagation direction. This makes some trouble in adopting the upwind method compared with incompressible flow. There are different ways to adopt the upwind method. In the following, after the introductions to FVS and AUSM-type schemes, the new flux splitting scheme AUSM$^+$–FVS will be defined.

3.1. FVS scheme

To use the upwind method, the eigenvalue matrix $\mathbf{\Lambda}$ is divided into positive and negative parts in the FVS scheme. The matrix can be written as follows:

$$\mathbf{\Lambda} = \mathbf{\Lambda}^+ + \mathbf{\Lambda}^- \tag{10}$$

The eigenvalues λ_i^+ in $\mathbf{\Lambda}^+$ are all positive. On the contrary, λ_i^- in $\mathbf{\Lambda}^-$ are all negative. So the inviscid fluxes can be divided into positive fluxes and negative fluxes.

$$\begin{aligned}\mathbf{F}(\mathbf{U}) &= \mathbf{L}\Lambda\mathbf{R}\mathbf{U} = \mathbf{L}(\Lambda^+ + \Lambda^-)\mathbf{R}\mathbf{U} \\ &= \mathbf{A}^+\mathbf{U} + \mathbf{A}^-\mathbf{U} = \mathbf{F}^+(\mathbf{U}) + \mathbf{F}^-(\mathbf{U})\end{aligned} \tag{11}$$

For a given form of $\mathbf{F}^{\pm}(\mathbf{U})$, it is easy to calculate the positive and negative fluxes using the upwind method in the two directions, respectively.

There are different kinds of FVS schemes in which different forms of $\mathbf{F}^{\pm}(\mathbf{U})$ are used. Among them, one scheme which can be regarded as an improvement of Van Leer's FVS is expressed as follows [21, 22]:

$$F_1^{\pm} = \pm\frac{1}{4}\rho a(M \pm 1)^2, F_2^{\pm} = F_1^{\pm}[u - \frac{p}{\rho a^2}(u \mp 2a)], F_3^{\pm} = F_1^{\pm}H, (|M| \le 1) \tag{12}$$

here, $F_1^{\pm}, F_2^{\pm}, F_3^{\pm}$ are the components of $\mathbf{F}^{\pm}$. Eq. (12) can be rewritten as:

$$\begin{aligned}F_1^{\pm} &= \pm\frac{1}{4}(M \pm 1)^2 a\rho \\ F_2^{\pm} &= \pm\frac{1}{4}(M \pm 1)^2 a\rho u - F_1^{\pm}\frac{u \mp 2a}{\rho a^2}p \\ &= \pm\frac{1}{4}(M \pm 1)^2 a\rho u + \frac{1}{4}(M \pm 1)^2(2 \mp M)p \\ F_3^{\pm} &= \pm\frac{1}{4}(M \pm 1)^2 a\rho H,\ (|M| \le 1)\end{aligned} \tag{13}$$

Thus, $\mathbf{F}^{\pm}$ can be calculated as:

$$\mathbf{F}^{\pm} = M^{\pm}a\mathbf{\Phi} + P^{\pm}\mathbf{P} \tag{14}$$

Where $\mathbf{\Phi} = [\rho, \rho u, \rho H]^T$, $\mathbf{P} = [0, p, 0]^T$, and $M^{\pm}$, $P^{\pm}$ can be calculated as:

$$M^{\pm} = \begin{cases} \pm\frac{1}{4}(M \pm 1)^2, |M| \le 1 \\ \frac{1}{2}(M + |M|), |M| > 1 \end{cases} \tag{15}$$

$$P^{\pm} = \begin{cases} \frac{1}{4}(M \pm 1)^2(2 \mp M), |M| \le 1 \\ \frac{1}{2}(1 \pm \mathrm{sign}(M)), |M| < 1 \end{cases} \tag{16}$$

Eqs. (14)–(16) define the positive and negative fluxes of the FVS scheme based on [21, 22]. Using the above equations, the inviscid fluxes at the interface can be calculated as $\mathbf{F}_{1/2} = \mathbf{F}_{1/2}^+ + \mathbf{F}_{1/2}^- = \mathbf{F}_{1/2}^c + \mathbf{F}_{1/2}^p$.here

$$\mathbf{F}_{1/2}^c = a_L M_L^+ \mathbf{\Phi}_L + a_R M_R^- \mathbf{\Phi}_R \tag{17}$$

$$\mathbf{F}_{1/2}^p = P_L^+ \mathbf{P}_L + P_R^- \mathbf{P}_R \tag{18}$$

3.2. AUSM+ scheme

When using the AUSM+ scheme to obtain the 1-D inviscid fluxes, the fluxes are divided into convective part and pressure part which can be written as follows:

$$\mathbf{F} = \begin{pmatrix} \rho \\ \rho u \\ \rho H \end{pmatrix} u + \begin{pmatrix} 0 \\ p \\ 0 \end{pmatrix} = \mathbf{F}^c + \mathbf{P} \tag{19}$$

The Jacobian matrix of $\mathbf{F}^c$ is

$$\mathbf{A}^c = \begin{pmatrix} 0 & 1 & 0 \\ -u^2 & 2u & 0 \\ -\gamma ue + (\gamma-1)u^3 & \gamma e - \frac{3}{2}(\gamma-1)u^2 & \gamma u \end{pmatrix} \tag{20}$$

The eigenvalues of $\mathbf{A}^c$ are

$$\lambda_1 = u, \lambda_2 = u, \lambda_3 = \gamma u \tag{21}$$

From the above equations, it can be seen that the eigenvalues have the same sign, which means that the waves have the same propagation direction. So at the interface, the inviscid fluxes can be calculated as:

$$\mathbf{F}_{1/2} = a_{1/2}(M_L^+ + M_R^-)\mathbf{\Phi}_{L/R} + P_L^+\mathbf{P}_L + P_R^-\mathbf{P}_R \tag{22}$$

The upwind variables can be decided as follows:

$$(\cdot)_{L/R} = \begin{cases} (\cdot)_L, & if\ M_{1/2} \geq 0 \\ (\cdot)_R, & otherwise \end{cases}, \tag{23}$$

where $M_{1/2}$ is the Mach number at the interface which can be calculated as $M_{1/2} = M_L^+ + M_R^-$. Here, $M^\pm$ and $P^\pm$ are calculated as:

$$M^\pm = \begin{cases} \pm\frac{1}{4}(M \pm 1)^2 \pm \frac{1}{8}(M^2-1)^2, & |M| \leq 1 \\ \frac{1}{2}(M + |M|), & |M| > 1 \end{cases} \tag{24}$$

$$P^\pm = \begin{cases} \frac{1}{4}(M \pm 1)^2(2 \mp M) \pm \frac{3}{16}M(M^2-1)^2, & |M| \leq 1 \\ \frac{1}{2}(1 \pm \mathrm{sign}(M)), & |M| < 1 \end{cases} \tag{25}$$

3.3. The hybrid splitting scheme: AUSM$^+$–FVS

In the FVS scheme, for adopting the upwind method, the eigenvalues are divided into positive part and negative part, so the inviscid fluxes are the sum of two different splitting fluxes. For each of the splitting fluxes, the upwind method can be adopted easily. As indicated above, the FVS schemes are very robust and can avoid the carbuncle phenomenon, but these schemes have a very poor performance in solving the boundary layer region. In the AUSM+ scheme, the inviscid fluxes are divided into convective part and pressure part. For the convective part, the eigenvalues have the same sign. The AUSM+ scheme has a very good accuracy in the boundary layer, but it suffers from the carbuncle phenomenon. Here, the major idea of these two different splitting schemes are combined to construct the new scheme AUSM$^+$–FVS which hopefully can retain their advantages and eliminate their disadvantages.

First, similar to the AUSM+, the eigenvalue matrix $\mathbf{\Lambda}$ is divided into two different matrixes $\mathbf{\Lambda}_a$ and $\mathbf{\Lambda}_b$:

$$\mathbf{\Lambda}_a = \begin{bmatrix} u & 0 & 0 \\ 0 & u & 0 \\ 0 & 0 & \gamma u \end{bmatrix}, \mathbf{\Lambda}_b = \begin{bmatrix} 0 & 0 & 0 \\ 0 & -a & 0 \\ 0 & 0 & a + (1-\gamma)u \end{bmatrix} \tag{26}$$

The matrix $\mathbf{\Lambda}_a$ itself can also be divided into two parts $\mathbf{\Lambda}_{a1}$ and $\mathbf{\Lambda}_{a2}$. Here $\mathbf{\Lambda}_{a1} = \beta\mathbf{\Lambda}_a$ and $\mathbf{\Lambda}_{a2} = (1-\beta)\mathbf{\Lambda}_a, (0 \leq \beta \leq 1)$. So the matrix $\mathbf{\Lambda}$ can be written as:

$$\mathbf{\Lambda} = \mathbf{\Lambda}_{a1} + \mathbf{\Lambda}_{a2} + \mathbf{\Lambda}_b \tag{27}$$

Thus, the inviscid fluxes can be divided into three parts. The fluxes which are corresponding to $\mathbf{\Lambda}_{a2}$ and $\mathbf{\Lambda}_b$ can be calculated by the method used in AUSM+ (Eq. 22). The sum of these two fluxes can be written as:

$$\mathbf{F}_{a2} + \mathbf{F}_b = (1-\beta)a_{1/2}(M_L^+ + M_R^-)\mathbf{\Phi}_{L/R} + P_L^+\mathbf{P}_L + P_R^-\mathbf{P}_R \tag{28}$$

Second, similar to FVS scheme, the matrix $\mathbf{\Lambda}_{a1}$ is divided into positive part and negative part ($\mathbf{\Lambda}_{a1} = \mathbf{\Lambda}_{a1}^{+} + \mathbf{\Lambda}_{a1}^{-}$). So, the fluxes which are corresponding to $\mathbf{\Lambda}_{a1}$ can be obtained using Eq. (17) of the FVS. To integrate it into the above equation, a_L and a_R in Eq. (17) are replaced by $a_{1/2}$. Thus, the fluxes can be written as:

$$\mathbf{F}_{a1} = \beta a_{1/2}(M_L^{+}\mathbf{\Phi}_L + M_R^{-}\mathbf{\Phi}_R) \tag{29}$$

Third, by summing up the above three components through some manipulations, it can be shown that the inviscid fluxes at the interface of the new hybrid scheme can be calculated as:

$$\mathbf{F}_{1/2} = \mathbf{F}_{a1} + \mathbf{F}_{a2} + \mathbf{F}_b = a_{1/2}(\overline{M}_L^{+}\mathbf{\Phi}_L + \overline{M}_R^{-}\mathbf{\Phi}_R) + P_L^{+}\mathbf{P}_L + P_R^{-}\mathbf{P}_R \tag{30}$$

where if $M_{1/2} \geq 0$, then

$$\begin{aligned} \overline{M}_L^{+} &= M_L^{+} + (1-\beta)M_R^{-} \\ \overline{M}_R^{-} &= \beta M_R^{-} \end{aligned} \tag{31}$$

if $M_{1/2} < 0$, then

$$\begin{aligned} \overline{M}_L^{+} &= \beta M_L^{+} \\ \overline{M}_R^{-} &= M_R^{-} + (1-\beta)M_L^{+} \end{aligned} \tag{32}$$

where $M^{\pm}$ and $P^{\pm}$ are calculated by Eqs. (24) and (25).

The parameter β in Eqs. (31) and (32) should be carefully determined. It should meet the following requirement: in the boundary layer region, the new scheme should be similar to AUSM+ to retain a good accuracy. In the shock region, the new scheme should be similar to FVS. After several preliminary computations, we propose the following equation for determining its value:

$$\beta = \begin{cases} 1 & M_\beta > \eta \\ \exp[-\frac{(M_\beta - \eta)^2}{2\alpha^2}] & M_\beta \leq \eta \end{cases} \tag{33}$$

where $\eta = 0.5$ and $\alpha = 0.1$. M_β is the local Mach number at the interface. For three-dimensional situation, M_β can be calculate as:

$$M_\beta = 0.5(\sqrt{u_L^2 + v_L^2 + w_L^2}/a_{1/2} + \sqrt{u_R^2 + v_R^2 + w_R^2}/a_{1/2}). \tag{34}$$

From Eq. (33), it can be obtained $\beta(M_\beta = 0) = 3.727 \times 10^{-6}$ and $\beta(M_\beta \geq 0.5) = 1$. So when $M_\beta = 0$, this new scheme is very similar to AUSM+, and it is equal to FVS near the shock region. In the following presentation, this new scheme is called as AUSM^{+}–FVS.

4. Numerical experiments

In this section, the proposed new splitting scheme (AUSM^{+}–FVS) is applied to simulate five well-known compressible fluid flows to demonstrate its robustness and accuracy

4.1. One-dimensional Riemann problem

A Riemann problem consists of an initial value problem described by a conservation equation. At initial time, the field is usually separated by some constant states. Because the properties such as shocks and rarefaction waves appear as characteristics in the solution, the Riemann problem is very useful for examining the numerical schemes of solving the Euler conservation equations.

The one-dimensional Riemann problem is commonly used to study the performance of numerical schemes. In the test, the computational domain contains two constant states $(\rho, u, p)_L$ and $(\rho, u, p)_R$ at initial time. Here, this one-dimensional test is implemented in the domain $x \in [-1, 1]$. The initial conditions are

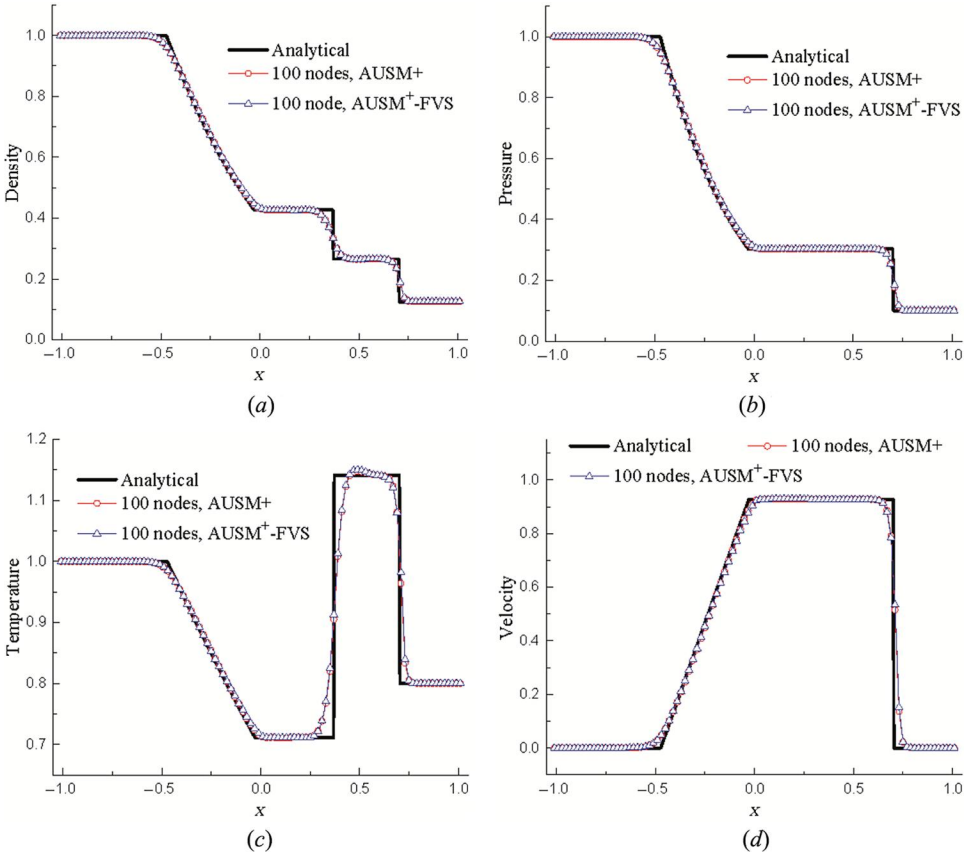

Figure 1. Numerical results of one-dimensional Riemann problem. (*a*) Density, (*b*) pressure, (*c*) temperature, and (*d*) velocity.

$$\begin{aligned}(\rho, u, p)_L &= (1, 0, 1), x \in [-1, 0] \\ (\rho, u, p)_R &= (0.125, 0, 0.1), x \in [0, 1]\end{aligned} \tag{35}$$

The second-order Runge–Kutta scheme is adopted to advance the transient term of Euler equation. Totally, 100 nodes are used to discretize the domain. Spatial accuracy is of second order. The profiles of density, pressure, temperature, and velocity which are obtained using AUSM$^+$–FVS and AUSM+ at time 0.4 are illustrated in Figure 1. For comparison, the theoretical solution is also shown in the figure with the black line. From the figure, it can be seen that the results obtained by the new scheme are very close to those obtained by the AUSM+ scheme. From the above results, it can be found that AUSM$^+$–FVS can capture the 1-D discontinuities accurately.

4.2. Two-dimensional Riemann problem

In this test, two cases are solved in a 2-D domain $x \in [0, 1] \times y \in [0, 1]$. The initial conditions are as follows [23]:

$$\text{Case1} : (p, \rho, u, v) = \begin{cases} (0.4, 0.5313, 0, 0), & x \in (0.5, 1] \text{ and } y \in (0.5, 1] \\ (1, 1, 0.7276, 0), & x \in [0, 0.5) \text{ and } y \in (0.5, 1] \\ (1, 0.8, 0, 0), & x \in [0, 0.5) \text{ and } y \in [0, 0.5) \\ (1, 1, 0, 0.7276), & x \in (0.5, 1] \text{ and } y \in [0, 0.5) \end{cases} \tag{36}$$

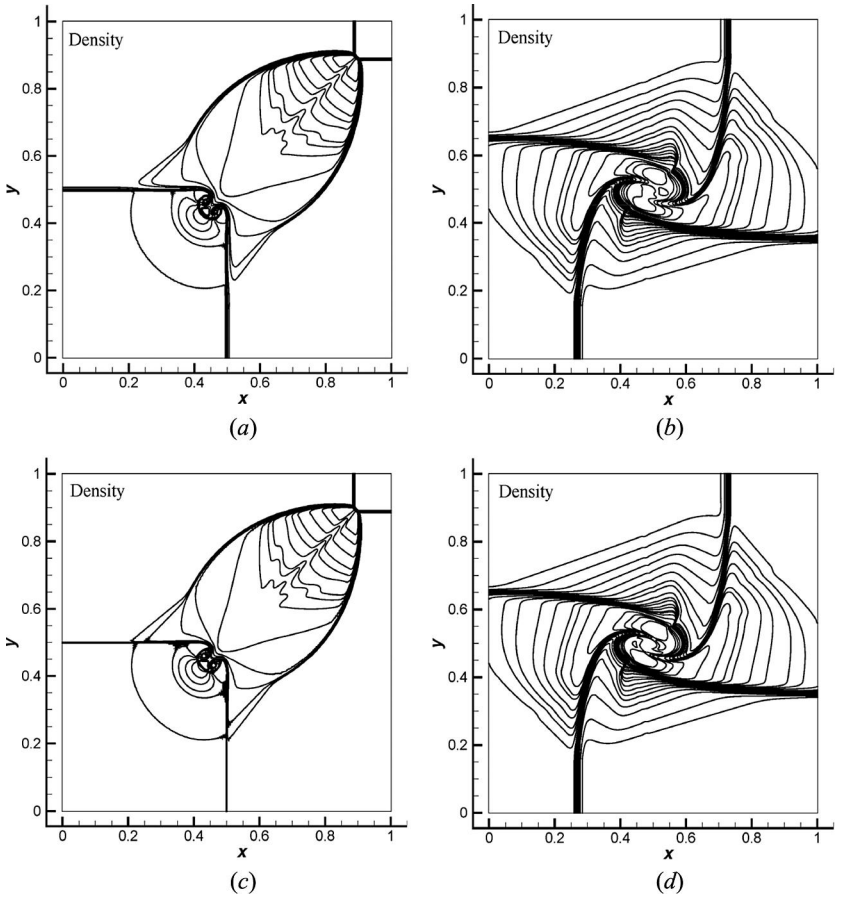

Figure 2. Density distributions of two-dimensional Riemann problems. (*a*) Case 1, AUSM$^+$–FVS, time = 0.25. (*b*) Case 2, AUSM$^+$–FVS, time = 0.3. (*c*) Case 1, AUSM+, time = 0.25. (*d*) Case 2, AUSM+, time = 0.3.

$$\text{Case2}: (p, \rho, u, v) = \begin{cases} (1.0, 1.0, 0.75, -0.5), & x \in (0.5, 1] \text{ and } y \in (0.5, 1] \\ (1.0, 2.0, 0.75, 0.5), & x \in [0, 0.5) \text{ and } y \in (0.5, 1] \\ (1.0, 1.0, -0.75, 0.5), & x \in [0, 0.5) \text{ and } y \in [0, 0.5) \\ (1.0, 3.0, -0.75, -0.5), & x \in (0.5, 1] \text{ and } y \in [0, 0.5) \end{cases} \tag{37}$$

A structured grid system with 400×400 points is used in this test. The simulation are second-order accuracy in space. The methods of advancing the transient term are also the second-order Runge–Kutta scheme. The density distributions at two time instants are displayed in Figure 2. As can be seen from the figure, the complex flow features are well predicted by AUSM$^+$–FVS (Figures 2(*a*) and 2(*b*)). The results are very similar with those obtained by AUSM+ (Figures 2(*c*) and 2(*d*)). It is very obvious that this new scheme has good capability of capturing the discontinuities.

4.3. Double-mach reflection problem

This test is particularly adopted to verify whether the proposed scheme can eliminate the kinked Mach stem. As mentioned before, many high-accuracy upwind schemes can produce kinked Mach stem in the numerical simulation of this problem. The problem is schematically shown in Figure 3. In the problem, an oblique shock of Ma = 10 hits the bottom reflecting wall.

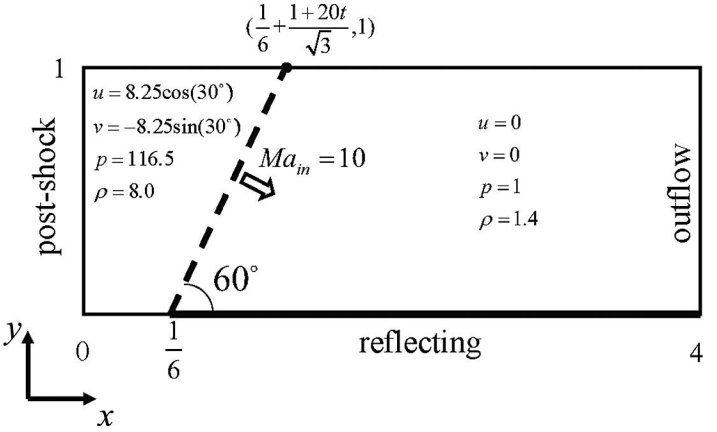

Figure 3. Schematic diagram of double-Mach reflection problem.

The computational domain is $x \in [0,4] \times y \in [0,1]$. At the initial time, the shock is inclined to the bottom wall with an 60° angle. The intersection of shock line and bottom boundary line is $(1/6, 0)$. Therefore, the initial conditions are [24]

$$(\rho, u, v, p) = \begin{cases} (8.0, 8.25\cos(30^\circ), -8.25\sin(30^\circ), 116.5), x < \frac{1}{6} + \frac{y}{\sqrt{3}} \\ (1.4, 0, 0, 1.0), x \geq \frac{1}{6} + \frac{y}{\sqrt{3}} \end{cases} \tag{38}$$

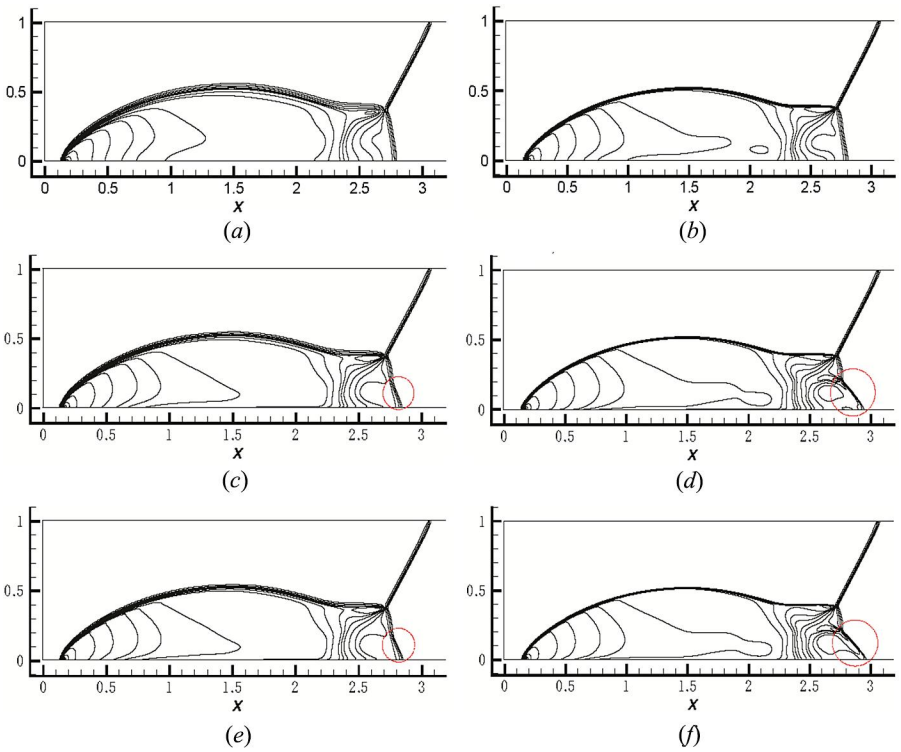

Figure 4. Density contours of double-Mach reflection problem. (*a*) AUSM$^+$–FVS, grid 400 × 100; (*b*) AUSM$^+$–FVS, grid 400 × 400; (*c*) AUSMPW+, grid 400 × 100; (*d*) AUSMPW+, grid 400 × 400; (*e*) AUSM+, grid 400 × 100; and (*f*) AUSM+, grid 400 × 400.

The left and the nonreflective bottom ($x \in [0, 1/6]$) boundaries are of postshock condition. The bottom boundary for $x \geq 1/6$ is a reflecting wall. The right boundary is zero-gradient condition. The intersection of the shock and the top boundary at time t is $\left(\frac{1}{6} + \frac{1+20t}{\sqrt{3}}, 1\right)$.

Two grids are used in this simulation. One is 400×100 and the other is 400×400. For the transient term, the second-order Runge–Kutta scheme is used. As mentioned above (Section 1), the shock anomalies occur more often in first-order integration method. Here, the first-order accuracy is achieved in space. The interface fluxes are calculated by AUSM$^+$–FVS, AUSM+, and AUSMPW+ for comparison. The density contours at time 0.2 are displayed in Figure 4. As seen from the figure, when the grid system is 400×100, the result obtained by AUSM$^+$–FVS does not show the instability phenomenon, while the kinked Mach stem phenomenon (marked by red circle in Figure 4) slightly exists in those results of AUSM+ and AUSMPW+.

When the grid system is 400×400, the results obtained by AUSM+ and AUSMPW+ both show the kinked Mach stem phenomenon (marked by red circle in Figure 4), but this phenomenon has not been found in the result obtained by the new scheme. It can be clearly seen that AUSM$^+$–FVS is more robust than the AUSM+ and AUSMPW+ in this test.

4.4. Odd–even problem

This test was first proposed by Quirk [12] to demonstrate the shock instability. In the test, a planar shock with Mach 6 moves from the left to the right in a duct. The inlet Mach number 6 is defined as $u_{\text{shock}}/a_{\text{up}}$ where u_{shock} is the speed of the shock, a_{up} is the sound speed of the upstream flow. In this test, the domain is $x \in [0, 1000] \times y \in [0, 25]$. The computational mesh is uniform with 800×20 cells. To add some perturbations, the centerline of the mesh is determined as follows:

$$y_{i,j_{\text{mid}}} = y_{j_{\text{mid}}} + (-1)^i \times 10^{-2} \tag{39}$$

where i is the grid subscript in x-direction.

Figure 5 is the schematic diagram of this treatment. The domain is initialized with $\rho = 1.4, p = 1.0, u = v = 0$. The left boundary is set to postshock values which can be calculated using Rankine–Hugoniot equations. The right boundary is just a simple extrapolation. The top and bottom boundaries are both the wall condition (normal velocity is zero). The new scheme and AUSMPW+, AUSM+ are used to obtain the fluxes of interface. The CFL number is set to 0.5 for these schemes. All the computations are performed in the first-order accuracy in space. At time $t =$ 150, the density contours obtained by AUSMPW+, AUSM+, and AUSM$^+$–FVS are shown in Figures 6(*a*)–(*c*), respectively. In those contours, there are 20 contour levels varying from 1.5 to 7.5.

From the figure, it can be seen that AUSMPW+ and AUSM+ both have the instability phenomenon. However, AUSM$^+$–FVS successfully preserves the initial shock.

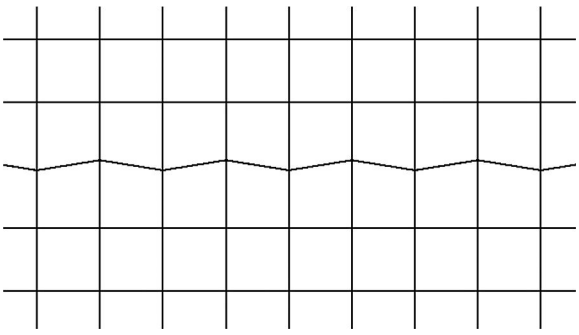

Figure 5. Schematic diagram of the grid.

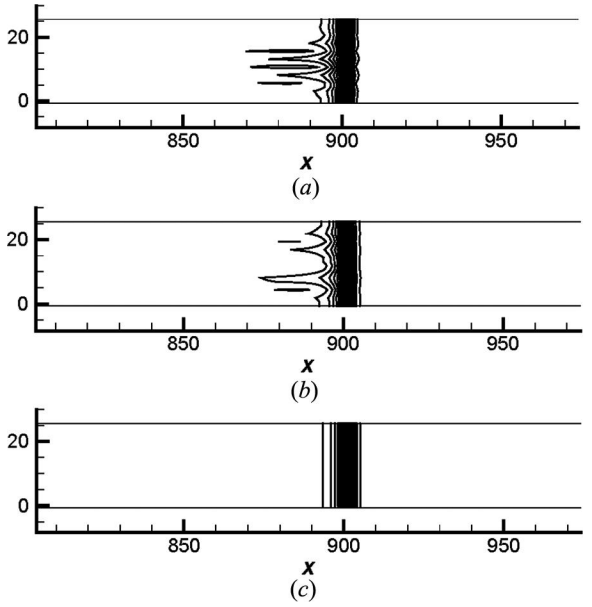

Figure 6. Density contours of odd–even problem. (*a*) AUSM+, (*b*) AUSMPW+, and (*c*) AUSM^{+}–FVS.

4.5. Blunt body problem

4.5.1. Mach 20 inviscid flow over a cylinder

This is a well-known test [25] to examine the performance of a scheme in regard to carbuncle instability. The free stream Mach number is 20. A structured grid with 40×1020 (radial $\times$ circumferential) cells is used in this simulation. The initial conditions are $\rho = 1.4, p = 1.0, u = 20, v = 0$. First-order spatial accuracy is used for all the schemes. The density contours obtained by three schemes are illustrated in Figure 7. As shown in this figure, AUSMPW+ and AUSM+ both produce the instability in this test. But the carbuncle phenomenon is not found in the result obtained by this new scheme.

To further verify the robustness of this new scheme, some perturbations are then added on the centerline of the above grid as follows:

$$\theta_{i,\mathrm{jmid}} = \theta_{\mathrm{jmid}} + (-1)^{i} \times (2 \times 10^{-2} \Delta\theta) \tag{40}$$

Here, $\Delta\theta = 180^{\circ}/1020$. Figure 8 is the schematic diagram of this treatment. The density contours obtained using this grid system are shown in Figure 9. It can be seen that AUSM^{+}–FVS is very robust even with the distorted cells.

4.5.2. Mach 15 viscous flow over a cylinder

To examine the accuracy of the new scheme, this viscous flow test is used for which reference solutions are available for comparison. This test was once adopted in the work done by Lee and Rho [26] to examine the accuracy of AUSM+ scheme. The test conditions which are taken from the run 89 in references [27] are as follows:

$$Ma_{\infty} = 15.13,\ T_{\infty} = 86.5\ \mathrm{K},\ P_{\infty} = 2.205\ \mathrm{Pa},\ T_{w} = 297.5\ \mathrm{K}$$
$$u_{\infty} = 2821.83\mathrm{m/s}, \mathrm{cylinderradius}: r = 0.0381\mathrm{m}$$

In this test, the dynamic viscosity of the air is determined by the Sutherland formula. The thermal conductivity of air can be calculated as $\lambda_f = c_p \mu / Pr$. The Prandtl number Pr takes the

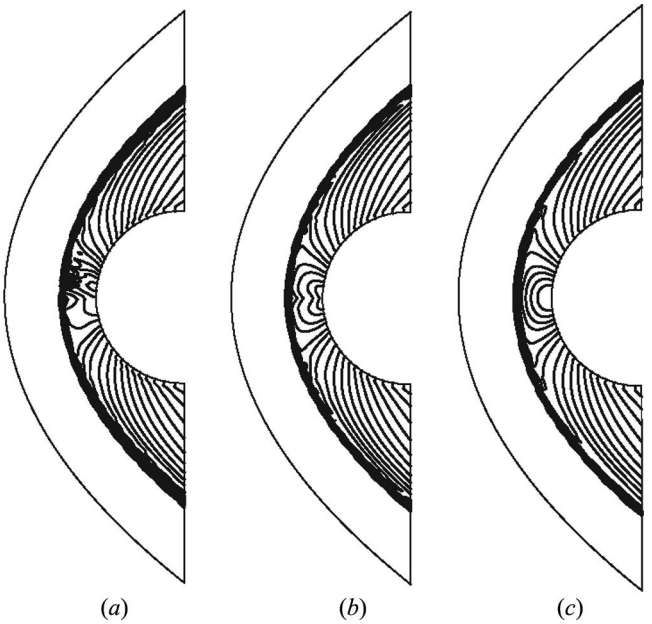

Figure 7. Density contours of flow over a cylinder with Ma = 20. (*a*) AUSM+, (*b*) AUSMPW+, and (*c*) AUSM^{+}–FVS.

value 0.72. The grid system is a structured one with 61 × 61 cells. The second-order Runge–Kutta scheme is adopted to advance the transient term. In space, the second-order accuracy is obtained by the reconstruction of primitive variables. In Figure 10, the curves of wall heat fluxes varying with the degrees from centerline are shown. The black line represents the results based

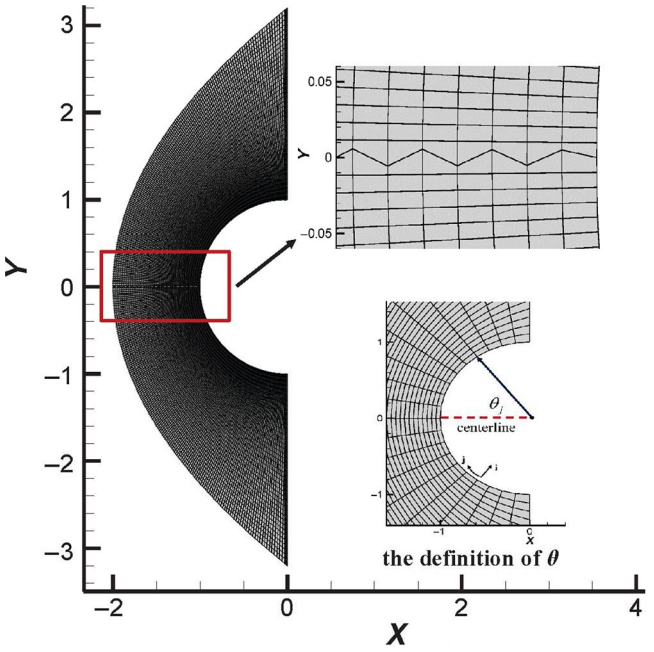

Figure 8. Schematic diagram of the distorted grid.

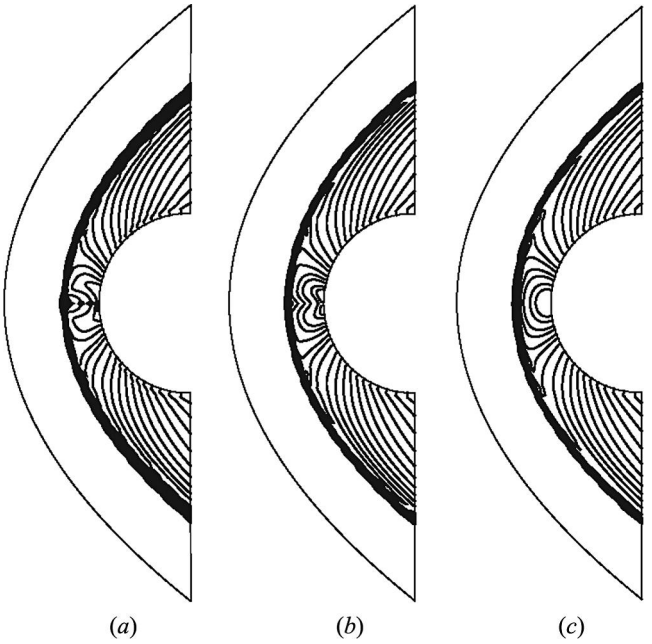

Figure 9. Density contours of flow over a cylinder with Ma = 20 and distorted grid. (*a*) AUSM+, (*b*) AUSMPW+, and (*c*) AUSM^{+}–FVS.

on Fay–Riddell theory from [27]. From the figure, it can be seen that the results obtained by AUSM^{+}–FVS are very close to those obtained by AUSM+ and AUSMPW+. The good accuracy of AUSM^{+}–FVS in this test is consistent with the theoretical analysis that the hybrid scheme is very similar to AUSM+ in the boundary layer region (Section 3.3). Because of the high numerical diffusion, the results obtained by FVS are very far from those obtained by the above three schemes.

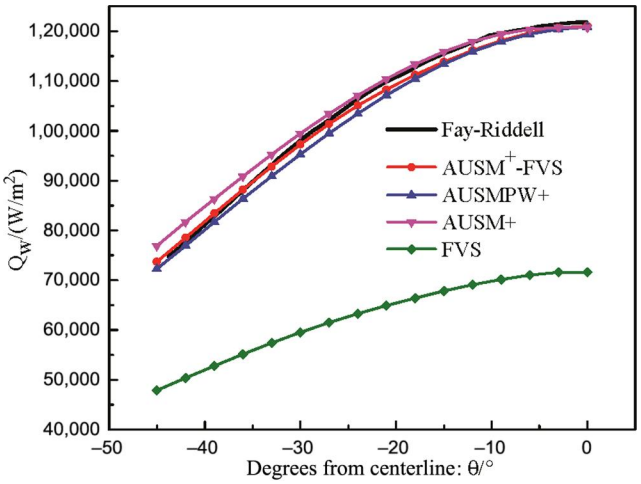

Figure 10. Wall heat flux distributions.

5. Conclusion

By dividing the eigenvalue matrix into three parts, a new scheme, called AUSM$^+$–FVS, which hybridizes the two different upwind schemes AUSM+ and FVS is proposed to calculate the inviscid fluxes of Euler/Navier–Stokes equations. Several numerical tests show that this new scheme can capture the discontinuities exactly. For the tests in which many low-diffusion upwind schemes produce the carbuncle phenomenon and shock instability, this new scheme shows its good robustness and can avoid those phenomena. For the viscous flow, this new scheme is very similar to AUSM+ in the boundary layer region and can obtain solutions with good accuracy in this region.

Funding

The present work was supported by the Key Project of International Joint Research of NSFC (51320105004) and the 111 Project (B16038).

References

[1] J. L. Steger and R. F. Warming, "Flux vector splitting of the inviscid gas-dynamic equations with application to finite-difference methods," *J. Comput. Phys.*, vol. 40, pp. 263–293, 1981. DOI: 10.1016/0021-9991(81)90210-2.
[2] B. van Leer, "Flux-vector splitting for the Euler equations,"Proceedings of 8th International Conference on Numerical Methods in Fluid Dynamics, Berlin, vol. 170, Springer, pp. 507–512, 1982.
[3] P. L. Roe, "Approximate Riemann solvers, parameter vectors, and difference schemes," *J. Comput. Phys.*, vol. 43, pp. 357–372, 1981. DOI: 10.1006/jcph.1997.5705.
[4] B. Einfeldt, "On Godunov-type methods for gas dynamics," *SIAM J. Numer. Anal.*, vol. 25, pp. 294–318, 1988. DOI: 10.1137/0725021.
[5] M. S. Liou and C. J. Steffen, "A new flux splitting scheme," *J. Comput. Phys.*, vol. 107, pp. 23–39, 1993. DOI: 10.1006/jcph.1993.1122.
[6] F. Qu, C. Yan, J. Yu, and D. Sun, "A new flux splitting scheme for the Euler equations," *Comput. Fluids*, vol. 102, pp. 203–214, 2014. DOI: 10.1016/j.compfluid.2014.07.004.
[7] M. S. Liou, "A sequel to AUSM: AUSM+," *J. Comput. Phys.*, vol. 129, pp. 364–382, 1996. DOI: 10.1006/jcph.1996.0256.
[8] Y. Wada and M. S. Liou, "A flux splitting scheme with high-resolution and robustness for discontinuities,"AIAA Paper 94–0083. Washington, DC: AIAA Press, 1994.
[9] K. H. Kim, C. Kim, and O.-H. Rho, "Methods for the accurate computations of hypersonic flows I. AUSMPW+ scheme," *J. Comput. Phys.*, vol. 174, pp. 38–80, 2001. DOI: 10.1006/jcph.2001.6873.
[10] M. S. Liou, "A sequel to AUSM, part II: AUSM$^+$-up for all speeds," *J. Comput. Phys.*, vol. 214, pp. 137–170, 2006. DOI: 10.1016/j.jcp.2005.09.020.
[11] K. Peery and S. Imlay, "Blunt-body flow simulations," AIAA Paper 88–2904. Washington, DC: AIAA Press, 1988.
[12] J. J. Quirk, "A contribution to the great Riemann solver debate," *Int. J. Numer. Methods Fluids*, vol. 18, pp. 555–574, 1994. DOI: 10.1007/978-3-642-60543-7_22.
[13] M. Pandolfi and D. D'Ambrosio, "Numerical instabilities in upwind methods: Analysis and cures for the "Carbuncle" phenomenon," *J. Comput. Phys.*, vol. 166, pp. 271–301, 2001. DOI: 10.1006/jcph.2000.6652.
[14] M. S. Liou, "Mass flux schemes and connection to shock instability," *J. Comput. Phys.*, vol. 160, pp. 623–648, 2000. DOI: 10.1006/jcph.2000.6478.
[15] J. Gressier and J. M. Moschetta, "Robustness versus accuracy in shock-wave computations," *Int. J. Numer. Methods Fluids*, vol. 33, pp. 313–332, 2000. DOI: 10.1002/1097-0363(20000615)33:3<313::aid-fld7>3.3.co;2-5.
[16] M. V. Ramalho, J. H. A. Azevedo, and J. L. F. Azevedo, "Further investigation into the origin of the carbuncle phenomenon in aerodynamic simulations," Proceedings of 49th AIAA Aerospace Sciences Meeting, Orlando, Florida, 2011.
[17] K. Xu, "Gas evolution dynamics in Godunov-type schemes and analysis of numerical shock instability." NASA Langley Research Center, Hampton, VA, Rept. 99–6, 1999.
[18] V. Elling, "The carbuncle phenomenon is incurable," *ACTA Math. Sci.*, vol. 29, pp. 1647–1656, 2009. DOI: 10.1016/s0252-9602(10)60007-0.
[19] R. W. MacCormack, "Carbuncle computational fluid dynamics problem for blunt-body flows," *J. Aerosp. Inform. Syst.*, vol. 10, pp. 229–239, 2013. DOI: 10.2514/1.53684.
[20] W. Xie, H. Li, Z. Tian, and S. Pan, "A low diffusion flux splitting method for inviscid compressible flows," *Comput. Fluids*, vol. 112, pp. 83–93, 2015. DOI: 10.1016/j.compfluid.2015.02.004.
[21] M. S. Liou, B. V. Leer, and J. S. Shuen, "Splitting of inviscid fluxes for real gases," *J. Comput. Phys.*, vol. 87, pp. 1–24, 1990. DOI: 10.1016/0021-9991(89)90195-2.

[22] B. van Leer, "Flux-vector splitting for the 1990s," Cleveland, OH: NASA, Rept. CP- 3078, 1991.
[23] A. Kurganov and E. Tadmor, "Solution of two-dimensional riemann problems for gas dynamics without Riemann problem solvers," *Numer. Method Part. Diff. Eq.*, vol. 18, pp. 584–608, 2002. DOI: 10.1002/num.10025.
[24] N. Kwatra, J. Su, J. T. Gretarsson, and R. Fedkiw, "A method for avoiding the acoustic time step restriction in compressible flow," *J. Comput. Phys.*, vol. 228, pp. 4146–4161, 2009. DOI: 10.1016/j.jcp.2009.02.027.
[25] J. C. Mandal and V. Panwar, "Robust HLL-type Riemann solver capable of resolving contact discontinuity," *Comput. Fluids*, vol. 63, pp. 148–164, 2012. DOI: 10.1016/j.compfluid.2012.04.005.
[26] J. H. Lee and O. H. Rho, "Accuracy of AUSM+ scheme in hypersonic blunt body flow calculation," AIAA Paper 98–1538. Washington, DC: AIAA Press, 1988.
[27] M. S. Holden, J. M. Kolly, and S. C. Martin, "Shock/shock interaction heating in laminar and low-density hypersonic flows,"AIAA Paper 96–1866. Washington, DC: AIAA Press, 1996.